Journal of Materials Chemistry A

COMMUNICATION

View Article Online
View Journal | View Issue

Cite this: J. Mater. Chem. A, 2015, 3, 5270

Received 8th January 2015
Accepted 27th January 2015

DOI: 10.1039/c5ta00165j

www.rsc.org/MaterialsA

PTC MWCNT/DI-water switchable composites†

Pengcheng Sun,[ab] Yun Huang,[b] Jun Yang,[b] Guoan Cheng[a] and Ruiting Zheng*[a]

Switchable electrical and thermal conductivities are desirable in many applications such as automatic regulation of building temperature, circuit protection, *etc.* In this paper, we study the electrical and thermal conductivities of multi-walled carbon nanotube (MWCNT)/DI-water composites *via* first order phase transition. We demonstrate that, with SDBS functionalized MWCNTs, the composites show unique positive temperature coefficient (PTC) electrical switching and negative temperature coefficient (NTC) thermal switching properties. Around 0 °C, the corresponding contrast ratio of electrical and thermal conductivities reaches 1250 and 3.58 times respectively.

Introduction

Brine rejection is a very interesting natural phenomenon in the course of salt solution freezing, which is caused by the big difference of salt solubility between liquid water and ice.[1] Brine rejection has obvious influences on the mechanical, biological and transport properties of the solution system.[2,3] One of the famous instances is the critical permeability phenomenon of sea ice.[4] Inspired by the rejection effects, transport properties of freezable suspensions have been studied recently. By dispersing graphite flakes, MWCNTs and SWCNTs into hexadecane and octadecane, electrical and thermal conductivity switchable composites are achieved.[5–8] During the freezing, the conductive nanoparticles are squeezed to the grain boundary of the organic crystals. Percolation networks and stress-generation during crystallization reduce the electrical and thermal contact resistances in composites, leading to large changes in the electrical and/or thermal conductivities. The contrast ratio of electrical conductivity (EC) and thermal conductivity (TC) of the switching composites reached 5 orders and 3.2 times respectively.[6,7] The reversible tuning of suspensions' electrical and thermal properties near room temperature by first-order phase transition opens a door for developing new thermosensitive materials with flexible critical temperatures, and also sparks the transport mechanism research of phase transition composites.[9–11]

So far, most of the organic fluid based composites have shown NTC effects; PTC effects have not been reported. In this paper, the electrical and thermal properties of MWCNT/deionized (DI) water composites were studied. We find that, for the first time, the EC of the sodium dodecyl benzene sulfonate (SDBS) functionalized MWCNT (S-MWCNT) aqueous suspensions show a unique PTC effect, but the TC of which still shows a NTC effect. The biggest EC and TC contrast around the water–ice transition point are 3 orders and 3.58 times respectively. The mechanism of the PTC effect in the S-MWCNT aqueous suspensions is investigated too.

Results and discussion

In this paper, we use high purity (>95%) short MWCNTs to fabricate the composites. Fig. 1a is the SEM image of raw MWCNTs (R-MWCNTs), which are uniformly dispersed on the Si substrate. The length of the R-MWCNTs is about 0.5–1 μm and the diameter is about 10–15 nm. High-resolution transmission electron microscopy (HRTEM) images indicate that the R-MWCNT has well defined multi-layered structure and smooth surface (Fig. 1b). After the 2 hours of acid treatment, several external layers of the R-MWCNT are damaged by the attack of the oxidative groups, but the structure of internal layers are well kept (Fig. 1c).[12] In contrast, the HRTEM image of the S-MWCNT shows a layer of amorphous structure attached on the surface of MWCNT. The thickness of the amorphous layer is about 1 nm (Fig. 1d), which may have resulted from the absorption of the SDBS.[13] Fig. 1e shows the Fourier Transform IR (FTIR) spectrum of R-MWCNTs, O-MWCNTs and S-MWCNTs, respectively. For R-MWCNTs, the peak at 1632 cm^{-1} corresponds to the C=C

[a]Key Laboratory of Radiation Beam Technology and Materials Modification of Ministry of Education, College of Nuclear Science and Technology, Beijing Normal University, Beijing 100875, P. R. China. E-mail: rtzheng@bnu.edu.cn

[b]State Key Laboratory of Multi-phase Complex Systems, Institute of Process Engineering, Chinese Academy of Sciences, Beijing 100190, P. R. China

† Electronic supplementary information (ESI) available: Descriptions of experimental methods and additional information. See DOI: 10.1039/c5ta00165j

stretching mode of the graphite structure.[14] The peaks at 1384 cm^{-1} and 3432 cm^{-1} come from the C–H bending mode and O–H stretching mode respectively,[15] which might have been caused by the surface adsorption of hydrocarbon and water contamination.[14,15] After oxidative treatment, additional peaks at 1706 cm^{-1} and 1200 cm^{-1} appeared on the O-MWCNT samples, which may be due to the stretching mode of C═O and C–O. For S-MWCNT samples, the peaks at 2916 cm^{-1}, 2848 cm^{-1} and 1443 cm^{-1} come from the C–H stretching modes and bending modes of the SDBS. The peak around 1170 cm^{-1} should be caused by S–O mode.[16,17] The FTIR results confirm that the O-MWCNTs and S-MWCNTs are covered by the oxidative groups and SDBS respectively.

Dispersion of MWCNTs in aqueous media has been substantially studied in previous research;[13,18,19] surface functionalization is found to be an effective way to get stable MWCNT suspensions.[20] However, the re-dispersion properties of nano-materials in water have been barely studied, which are very important for the phase transition nano-composites. In this paper, the microstructure of the dilute O-MWCNT and S-MWCNT DI-water composites (0.05% volume fraction) during the phase change is observed by an optical microscope, as shown in Fig. 2. In the liquid state, the distribution of O-MWCNTs in DI-water is relatively uniform. The sizes of most O-MWCNT clusters are several micrometers; a minority of big clusters tends to be tens of microns (Fig. 2a). The optical photo of a 0.2% v/v O-MWNT/DI-water suspension is shown in the inset picture of Fig. 2a; no phase separation is observed after one month of standing, which shows a good stability of the samples. The corresponding Zeta potential of O-MWNTs is measured to be −51.5 mV. After freezing and melting three times, the O-MWCNTs tend to agglomerate due to the repeated squeezing of the ice crystals, and the size of the clusters grows to about 100 microns (Fig. 2b). Obvious phase separation happens in the corresponding suspensions because of the settling of the big O-MWNT clusters (inset picture of Fig. 2b). In comparison, the S-MWCNTs show better dispersion in DI-water (Fig. 2c), the cluster size of S-MWCNTs is about several microns, and a few big clusters are observed. There is also no phase separation in the suspension after one month of standing (inset picture of Fig. 2c) too, and the corresponding Zeta potential of S-MWCNT is −60 mV. After re-melting three times, a majority of the S-MWCNT clusters are still well separated, and only a few S-MWCNT clusters grow to 10–20 microns (Fig. 2d). The 0.2% v/v S-MWCNT/DI-water suspension shows no phase separation

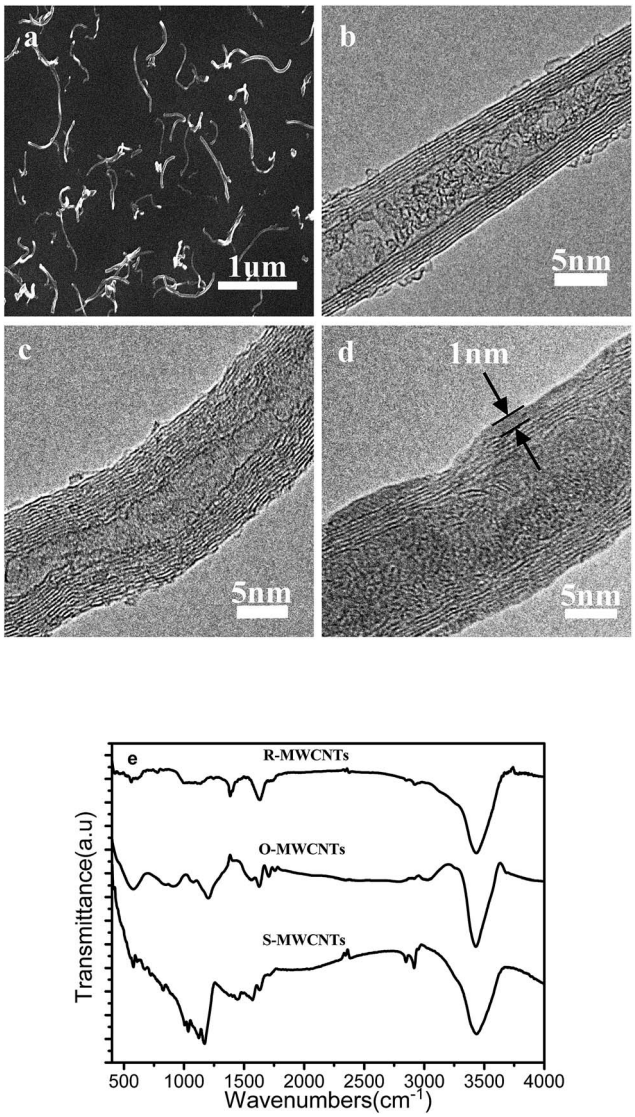

Fig. 1 (a) SEM image of the R-MWCNTs dispersed on the silicon substrate. (b–d) HRTEM images of the R-MWCNT, O-MWCNT and S-MWCNT respectively. (e) Mid-IR spectrum of the MWCNTs after different functionalization.

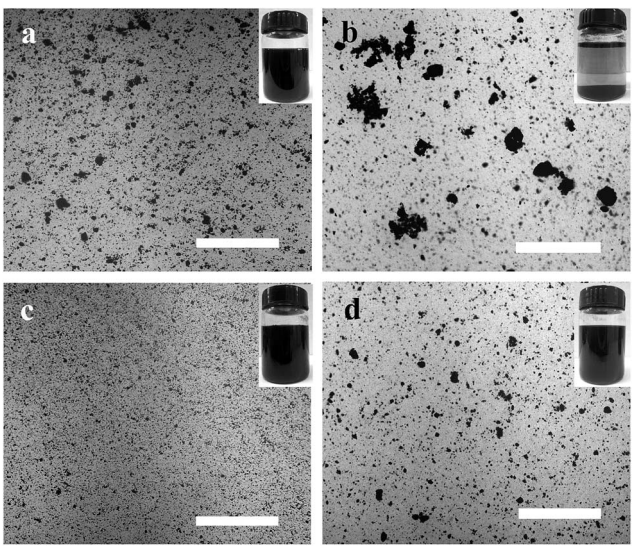

Fig. 2 Evolution of MWCNT microstructures in DI-water during the remelting process. (a and b) Images of 0.05% (v/v) O-MWCNT/DI-water composites in the original liquid state, after three times' re-melting, respectively. (c and d) Images of 0.05% (v/v) S-MWCNT/DI-water composites in the original liquid state, after three times' re-melting, respectively. The inset pictures are the digital photos of the corresponding suspensions. Scale bars in (a–d) all correspond to 200 μm.

after re-freezing three times (inset picture of Fig. 2d), which indicates better re-dispersion properties of S-MWCNT/DI-water suspensions than those of O-MWCNT/DI-water suspensions.

The different re-dispersion behaviors of the MWCNTs should be attributed to their different surface properties. As we know, O-MWCNTs are stabilized in DI-water by the electrostatic repulsion effects of the negatively charged oxidative groups.[19] Using SDBS as a surfactant, both electrostatic repulsion and steric repulsion that were caused by the longer alkyl chain work during the dispersion process.[13] When the composite freezes, the MWCNTs tend to be squeezed together under the strong pressure, which is much bigger than the corresponding repulsion force. As the ice crystals melt, the electrostatic repulsion force is insufficient to totally separate the MWCNTs. However, the steric effect of SDBS could push the S-MWCNTs away from each other, which is crucial for the good re-dispersion properties of MWCNT/DI-water composites. A similar re-dispersion mechanism is also found in the octadecylamine (ODA) functionalized MWCNT/hexadecane composite.[6]

The electrical and thermal transport properties of the S-MWCNT/DI-water composites around the phase transition point are shown in Fig. 3. In the liquid state, the EC of the composites varies a little with the change of temperature (Fig. 3a). From −0.5 to 0.5 °C, the EC increases several orders. After the DI-water is completely frozen, the EC stabilizes. In the liquid state, the EC increases from 4.4×10^{-2} S m^{-1} to 2.2×10^{-1} S m^{-1} with the S-MWCNT loading increase from 0.2% to 1% (5 °C). In the solid state, the corresponding EC also changes from 6.9×10^{-5} S m^{-1} (0.2%) to 3.7×10^{-4} S m^{-1} (1%) (−5 °C). The biggest EC contrast ratio between −5 °C and 5 °C is 1250 times at the volume fraction of 0.8%. TC of the S-MWCNT/DI-water composites as a function of temperature is shown in Fig. 3b. TC of the liquid composite changes little with the increase of temperature. In the course of freezing, the TC increases sharply. After the composite is completely frozen, the TC stabilizes too. For the S-MWCNT/DI-water composites, in both solid and liquid states, the TC of composites enhances with the increase of the S-MWCNT loading. The TC contrast ratio peaks 3.58 times at the volume fraction of 0.4% (v/v). The corresponding TC changes from 0.677 W mK^{-1} (liquid) to 2.43 W mK^{-1} (solid) as the temperature decreases from 5 °C to −5 °C.

The EC of the S-MWCNT/DI-water composites is higher in the liquid state, but lower in the solid state, which is in contrast to hexadecane based composites.[6,7] As efficient transport paths, MWCNTs could improve the transport properties of the composites in both liquid and solid states, but the distinct improvement will only happen when the MWCNT percolation structures form in the solid state.[21] That is why most oil based composites show a NTC EC effect. We conjecture that the SDBS plays an important role in the PTC EC switching properties of S-MWCNT/DI-water composites. Fig. 4 is the schematic diagram of the phase transition process in a S-MWCNT/DI-water composite. In the liquid composite, SDBS is ionized into $C_{18}H_{29}SO_3^{-1}$ and Na^{+1} in DI-water. Alkyl chains with SO_3^{-1} groups attach on the surface of S-MWCNTs, and the

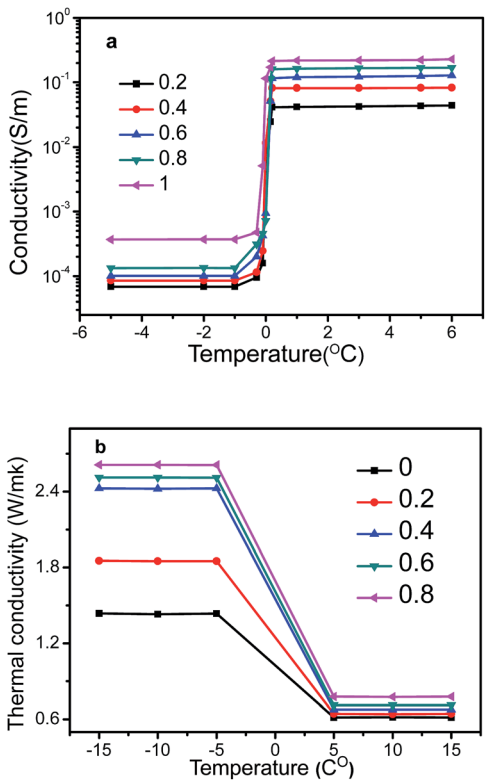

Fig. 3 Variation of EC and TC around the phase transition point. (a) EC of the MWCNT/DI-water composites with different CNT volume fractions. (b) TC of the MWCNT/DI-water composites with different CNT volume fractions.

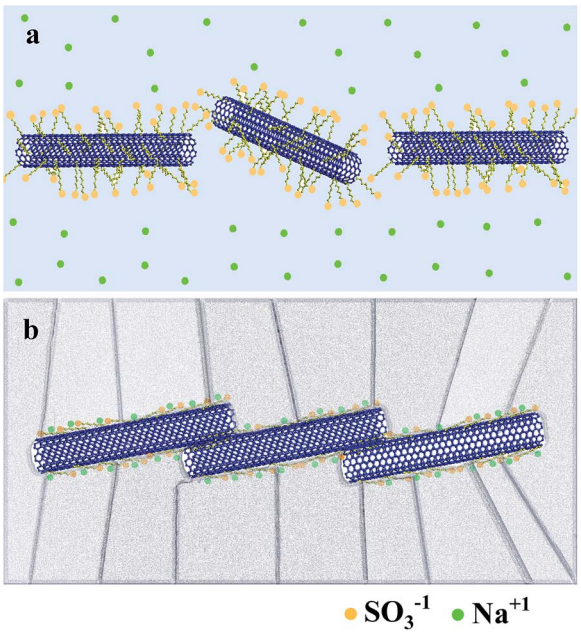

Fig. 4 Schematic diagram of the phase transition process in a S-MWCNT composite. (a) In the liquid state, S-MWCNTs are well dispersed with the help of surface functional groups. (b) In the frozen state, S-MWCNTs are squeezed to the grain boundary and form a transport network.

electrostatic repulsion and steric effect of the surfactant prevent the formation of S-MWCNT transport networks, which makes S-MWCNTs contribute less to EC (Fig. 4a). However, as an effective carrier, a large quantity of Na^{+1} ions should enhance the EC effectively in the liquid composites.[22] As shown in Fig. 4b, when the liquid composites change into solids, the Na^{+1} ions trend to migrate to the grain boundary of the ice crystals.[4,23] The electrical conductivity of the solid composites mainly comes from the S-MWCNT transport networks. The PTC effect in S-MWCNT/DI-water composites may be caused by the bigger EC that comes from the Na^{+1} transfer in the liquid state compared to the solid state.

EC of the liquid composites can be calculated by considering the molar conductivity and concentration of Na^{+1}. The EC of an electrolyte solution can be expressed as $k = \Lambda_m c$, in which k, Λ_m and c are the EC, molar conductivity and ion concentration of the solution, respectively. As the volume fraction of S-MWCNTs rises from 0.2% to 1%, the Na^{+1} concentration in liquid composites increases from 0.0241 mol L^{-1} to 0.121 mol L^{-1}. According to the report of Barthel *et al.*,[24] the molar conductivities of Na^{+1} in water at 5 °C are about 30.31×10^{-4} and 30.27×10^{-4} S m^2 mol^{-1} respectively at the concentrations of 0.0241 and 0.121 mol L^{-1}. The calculated EC of the liquid composites increased from 0.073 S m^{-1} (0.2%) to 0.366 S m^{-1} (1%). The EC of the liquid composites in our experiment changes from 0.044 S m^{-1} (0.2%) to 0.22 S m^{-1} (1%) at 5 °C. The theoretical and measured EC values are of the same order, which confirms that the EC of the liquid composites is mainly contributed by Na^{+1} transport. The difference of the EC values may be due to the S-MWCNT's blocking of Na^{+1} transport. In the solid composites, as the volume fraction of the S-MWCNTs increases from 0.2% to 0.8% (v/v), the transport networks are improved, which should be responsible for the increasing EC in the solid composites. The substantial enhancement of the EC from 0.8 to 1% (v/v) may be caused by the formation of the complete networks at high concentrations.[25] We think that the SDBS surfactant plays a vital role in the low EC of the solid composites. First, the π–π stacking of SDBS leads to disturbances of the π-electron delocalization of the S-MWCNT surfaces, which results in a significant deterioration of electrical properties of S-MWCNTs.[18] In another way, the amorphous SDBS coated on the surface of S-MWCNTs could cause the tremendous contact resistance between S-MWCNTs,[26,27] which further causes an obvious decrease of EC in S-MWCNT networks. Thus, the unique PTC EC properties of the S-MWCNT/DI-water composites are dominated by the transport mechanism of Na^{+1} in the liquid and solid composites respectively.

The largest TC contrast ratio of S-MWCNT/DI-water composites is 3.58 times between −5 °C and 5 °C, but the TC contrast ratio between pure DI-water and ice is only about 2.33 times. The migration of Na^{+1} contributes little to the thermal transport in liquid composites.[28] The TC enhancement in the solid state should be attributed to the faster phonon transport along the S-MWCNT networks.[29] That is why TC still shows a NTC effect. From 0.2 to 0.4% (v/v), the TC of the solid composites enhances to a great extent; we anticipate that the big enhancement is also due to the formation of S-MWCNT percolation networks. As we further increase the S-MWCNT volume fraction, the TC turns to be saturated.

The durability of the S-MWCNT/DI-water composites is evaluated by testing the cycling properties of the composites. The EC cycling properties of the 0.8% (v/v) S-MWCNT/DI-water composite are shown in Fig. 5a. In the first three cycles, the EC increases from 9.56×10^{-5} S m^{-1} to 1.34×10^{-4} S m^{-1} in the solid state and varies from 1.18×10^{-1} S m^{-1} to 1.67×10^{-1} S m^{-1} in the liquid state. The corresponding EC contrast ratio changes from 1234 to 1250 times. After recycling three times, the ratio of the EC becomes stable and approaches a constant (3 orders of magnitude). The TC cycling properties of 0.4% (v/v) S-MWCNT/DI-water composites are shown in Fig. 5b. In first three cycles, TC increases from 0.615 W mK^{-1} to 0.677 W mK^{-1} in the liquid state, but decreases from 2.67 W mK^{-1} to 2.43 W mK^{-1} in the solid state, and the corresponding TC contrast ratio decreases from 4.34 to 3.58 times. After the first three cycles, the TC becomes stable in both the liquid and the solid states, and the TC contrast ratio stabilizes at about 3.58 times.

The variation of EC and TC contrast ratio is thought to be closely related to the microstructure evolution of S-MWCNT composites during the freezing/remelting cycles. The growth of the S-MWCNT clusters in the re-melting process should be responsible for the change of EC and TC contrast ratio in the first three cycles. The growth of S-MWCNT clusters will be beneficial to the enhancement of EC in both liquid and solid composites, because the bigger clusters have higher efficiency for electron transport.[21,25] And the effective aggregation of S-MWCNTs is also helpful for TC increment in the liquid

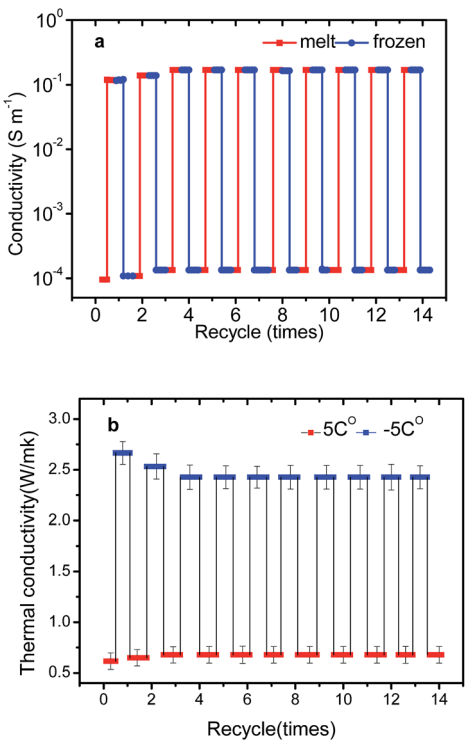

Fig. 5 Repetitive behavior tests of the S-MWCNT/DI-water composites. (a) EC and (b) TC.

composites.[30] But the worse dispersion of S-MWCNTs decreases TC in the solid composites, as other researchers also observed.[31,32] After the variation of the first three cycles, the structure of S-MWCNT clusters is stabilized, and the EC and TC contrast ratio stabilizes too.

Conclusions

In conclusion, switchable EC and TC transport properties of MWCNT/DI-water composites caused by phase transition are studied. The re-dispersion and transport properties of the composites are regulated by the surface functionalization of MWCNTs. By using SDBS functionalized MWCNTs, the biggest EC and TC contrast ratios of 3 orders and 3.58 times near the freezing point are achieved. The S-MWCNT/DI-water composites show unique PTC EC and NTC TC properties. The DI-water based switching composite shows high temperature coefficient, low cost and good durability, which have great potential in sensors, smart control, thermal storage and other related areas.

Acknowledgements

This work was supported by the National Basic Research Program of China (no. 2010CB832905), by the Key Scientific and Technological Project of the Ministry of Education of China (no. 108124), and partially by the National Natural Science Foundation of China (no. 11005059).

Notes and references

1 L. Vrbka and P. Jungwirth, *Phys. Rev. Lett.*, 2005, **95**, 148501.
2 A. Y. Shcherbina, L. D. Talley and D. L. Rudnick, *Science*, 2003, **302**, 1952–1955.
3 K. Caldeira and P. B. Duffy, *Science*, 2000, **287**, 620–622.
4 K. M. Golden, S. F. Ackley and V. I. Lytle, *Science*, 1998, **282**, 2238–2241.
5 T. Zhang and T. Luo, *ACS Nano*, 2013, **7**, 7592–7600.
6 P. Sun, Y. Wu, J. Gao, G. Cheng, G. Chen and R. Zheng, *Adv. Mater.*, 2013, **25**, 4938–4943.
7 R. Zheng, J. Gao, J. Wang and G. Chen, *Nat. Commun.*, 2011, **2**, 289.
8 S. Harish, K. Ishikawa, S. Chiashi, J. Shiomi and S. Maruyama, *J. Phys. Chem. C*, 2013, **117**, 15409–15413.
9 J. W. Gao, R. T. Zheng, H. Ohtani, D. S. Zhu and G. Chen, *Nano Lett.*, 2009, **9**, 4128–4132.
10 Z. Liu, R. Zou, Z. Lin, X. Gui, R. Chen, J. Lin, Y. Shang and A. Cao, *Nano Lett.*, 2013, **13**, 4028–4035.
11 B. Wang, J. Hao, Q. Li and H. Li, *Int. J. Therm. Sci.*, 2014, **83**, 89–95.
12 V. Datsyuk, M. Kalyva, K. Papagelis, J. Parthenios, D. Tasis, A. Siokou, I. Kallitsis and C. Galiotis, *Carbon*, 2008, **46**, 833–840.
13 M. F. Islam, E. Rojas, D. M. Bergey, A. T. Johnson and A. G. Yodh, *Nano Lett.*, 2003, **3**, 269–273.
14 U. J. Kim, C. A. Furtado, X. Liu, G. Chen and P. C. Eklund, *J. Am. Chem. Soc.*, 2005, **127**, 15437–15445.
15 E. Fuente, J. Menendez, M. Diez, D. Suarez and M. Montes-Moran, *J. Phys. Chem. B*, 2003, **107**, 6350–6359.
16 B. R. Priya and H. J. Byrne, *J. Phys. Chem. C*, 2007, **112**, 332–337.
17 Z. P. Xu and P. S. Braterman, *J. Mater. Chem.*, 2003, **13**, 268–273.
18 E. E. Tkalya, M. Ghislandi, G. de With and C. E. Koning, *Curr. Opin. Colloid Interface Sci.*, 2012, **17**, 225–232.
19 L. Jiang, L. Gao and J. Sun, *J. Colloid Interface Sci.*, 2003, **260**, 89–94.
20 H. Xie and L. Chen, *J. Chem. Eng. Data*, 2011, **56**, 1030–1041.
21 J. Li, P. C. Ma, W. S. Chow, C. K. To, B. Z. Tang and J. K. Kim, *Adv. Funct. Mater.*, 2007, **17**, 3207–3215.
22 G. Eisenman, *Anal. Chem.*, 1968, **40**, 310–320.
23 J. H. Kim, T. Shin, K. H. Jung and H. Kang, *ChemPhysChem*, 2005, **6**, 440–444.
24 M. Bešter-Rogač, R. Neueder and J. Barthel, *J. Solution Chem.*, 1999, **28**, 1071–1086.
25 W. Bauhofer and J. Z. Kovacs, *Compos. Sci. Technol.*, 2009, **69**, 1486–1498.
26 C. Li, E. T. Thostenson and T.-W. Chou, *Appl. Phys. Lett.*, 2007, **91**, 223114.
27 F. H. Gojny, M. H. G. Wichmann, B. Fiedler, I. A. Kinloch, W. Bauhofer, A. H. Windle and K. Schulte, *Polymer*, 2006, **47**, 2036–2045.
28 J. Eapen, J. Li and S. Yip, *Phys. Rev. Lett.*, 2007, **98**, 028302.
29 R. Zheng, J. Gao, J. Wang, S.-P. Feng, H. Ohtani, J. Wang and G. Chen, *Nano Lett.*, 2011, **12**, 188–192.
30 R. Prasher, P. E. Phelan and P. Bhattacharya, *Nano Lett.*, 2006, **6**, 1529–1534.
31 S. H. Song, K. H. Park, B. H. Kim, Y. W. Choi, G. H. Jun, D. J. Lee, B.-S. Kong, K.-W. Paik and S. Jeon, *Adv. Mater.*, 2013, **25**, 732–737.
32 J. E. Peters, D. V. Papavassiliou and B. P. Grady, *Macromolecules*, 2008, **41**, 7274–7277.

